Title

Integrin α2β1 regulates collagen I tethering to modulate hyperresponsiveness in reactive airway disease models

Journal

Journal of Clinical Investigation, 131(12)

ISSN

0021-9738

Authors

Liu, Sean
Ngo, Uyen
Tang, Xin-Zi
et al.

Publication Date

2021-06-15

DOI

10.1172/jci138140

Peer reviewed

Integrin $\alpha_2\beta_1$ regulates collagen I tethering to modulate hyperresponsiveness in reactive airway disease models

Sean Liu,[1] Uyen Ngo,[1] Xin-Zi Tang,[2,3,4] Xin Ren,[1] Wenli Qiu,[1] Xiaozhu Huang,[1] William DeGrado,[2,5] Christopher D.C. Allen,[2,3,6] Hyunil Jo,[2,5] Dean Sheppard,[1,2] and Aparna B. Sundaram[1]

[1]Lung Biology Center, Division of Pulmonary, Critical Care, Allergy and Sleep, Department of Medicine, [2]Cardiovascular Research Institute, [3]Sandler Asthma Basic Research Center, [4]Biomedical Sciences Graduate Program, [5]Department of Pharmaceutical Chemistry, and [6]Department of Anatomy, UCSF, San Francisco, California, USA.

Severe asthma remains challenging to manage and has limited treatment options. We have previously shown that targeting smooth muscle integrin $\alpha_5\beta_1$ interaction with fibronectin can mitigate the effects of airway hyperresponsiveness by impairing force transmission. In this study, we show that another member of the integrin superfamily, integrin $\alpha_2\beta_1$, is present in airway smooth muscle and capable of regulating force transmission via cellular tethering to the matrix protein collagen I and, to a lesser degree, laminin-111. The addition of an inhibitor of integrin $\alpha_2\beta_1$ impaired IL-13–enhanced contraction in mouse tracheal rings and human bronchial rings and abrogated the exaggerated bronchoconstriction induced by allergen sensitization and challenge. We confirmed that this effect was not due to alterations in classic intracellular myosin light chain phosphorylation regulating muscle shortening. Although IL-13 did not affect surface expression of $\alpha_2\beta_1$, it did increase $\alpha_2\beta_1$-mediated adhesion and the level of expression of an activation-specific epitope on the β_1 subunit. We developed a method to simultaneously quantify airway narrowing and muscle shortening using 2-photon microscopy and demonstrated that inhibition of $\alpha_2\beta_1$ mitigated IL-13–enhanced airway narrowing without altering muscle shortening by impairing the tethering of muscle to the surrounding matrix. Our data identified cell matrix tethering as an attractive therapeutic target to mitigate the severity of airway contraction in asthma.

Introduction

Asthma is a chronic inflammatory disease characterized by airway hyperresponsiveness, inflammation, and remodeling (1–3). Exaggerated airway narrowing in response to stimuli is the hallmark of airway hyperresponsiveness and is the underlying cause of recurrent episodes of wheezing and breathlessness that characterize asthma. The mainstays of management of asthma include medications aimed at decreasing inflammation and treating acute airway narrowing caused by excessive smooth muscle contraction. Two of the characteristic features of asthma are increased smooth muscle mass and the altered deposition of extracellular matrix surrounding smooth muscle bundles (4). Histological studies of the airways in patients with asthma show increased deposition of several extracellular matrix proteins, including collagens I, III, and VI (5); fibronectin; and laminin chains α1, α2, α3, α5, β1, β2, γ1, and γ2 (6–8). The role of endogenous matrix proteins in altering the physical properties of the airway wall and influencing the contraction of adjacent airway smooth muscle is incompletely understood.

To generate enough force to affect a change in the luminal area of the airway, smooth muscle cells must form a transmission pathway that integrates adjacent smooth muscle cells and the surrounding matrix. This connection is mediated in large part by members of the integrin family, which tether cells to the surrounding matrix via focal adhesions (9). Our group has shown that inhibition of integrin $\alpha_5\beta_1$–mediated tethering of smooth muscle to fibronectin has functional effects on force transmission ex vivo and in vivo (10). Furthermore, these effects occur without altering classical actin-myosin phosphorylation. It is not currently known whether other integrins are also capable of regulating force transmission in airway smooth muscle.

In this paper, we show that integrin $\alpha_2\beta_1$ is present on human airway smooth muscle and can regulate adhesion to the extracellular matrix protein collagen I and, to a lesser degree, laminin-111 (α1β1γ1). Inhibition of integrin $\alpha_2\beta_1$ impaired force generation ex vivo and airway hyperresponsiveness in vivo. Mechanistically, inhibition of integrin $\alpha_2\beta_1$ abrogated airway narrowing without altering smooth muscle shortening or the core actin-myosin machinery. These results underscore the important contribution of cellular tethering in regulating force transmission and identify the $\alpha_2\beta_1$ integrin as a therapeutic target for the treatment of exaggerated airway narrowing in asthma.

Results

Integrin $\alpha_2\beta_1$ regulates adhesion of smooth muscle to collagen I and laminin-111. We have previously shown that inhibition of integrin $\alpha_5\beta_1$ can impair force generation and the development of airway

Conflict of interest: AS, DS, HJ, and WD are co-inventors of a patent covering small-molecule α2β1 integrin inhibitors (Inhibitors of integrin alpha 2 beta 1 and methods of use; patent no. WO2019178248A1) and are funded by a grant from Shang-Pharma to commercially develop α2β1 integrin inhibitors.

Submitted: April 21, 2020; **Accepted:** May 5, 2021; **Published:** May 6, 2021.
Reference information: *J Clin Invest*. 2021;131(12):e138140.
https://doi.org/10.1172/JCI138140.

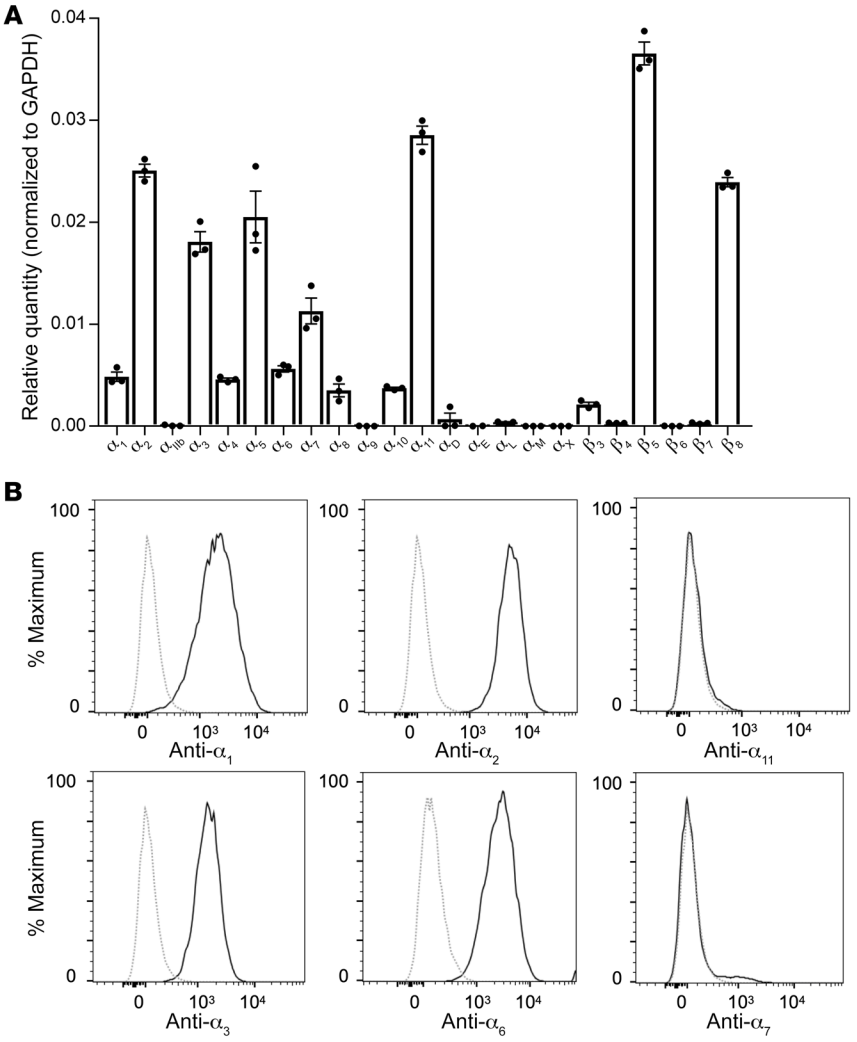

Figure 1. Integrin $\alpha_2\beta_1$ is expressed on human airway smooth muscle cells. (**A**) RNA was extracted from human airway smooth muscle cells grown in culture. Quantitative RT-PCR was performed to determine integrin expression; results were normalized to GAPDH expression. Data are the mean ± SEM. Experiment performed in triplicate with 3 biological replicates. (**B**) Human airway smooth muscle cells in suspension were labeled with primary antibodies specific for integrins α_1, α_2, α_3, α_6, α_7, and α_{11} and a secondary antibody conjugated to allophycocyanin (APC) or FITC. The cells were analyzed by flow cytometry and gated for live cells. The resultant population was analyzed for APC or FITC expression (black solid line). Human airway smooth muscle cells labeled with secondary antibody alone served as an unstained control (gray dashed line). Representative histograms of APC or FITC expression (MFI) versus cell count scaled to mode (percentage of maximum) are shown. Results verified with 3 biological replicates.

hyperresponsiveness without altering the core actin-myosin apparatus (10). We hypothesized that this effect was due to impaired tethering of hyperresponsive airway smooth muscle to fibronectin in the surrounding tissue, thus allowing muscle to shorten but reducing the degree to which shortening would result in narrowing of the airway lumen. It remains unknown whether other integrins, which mediate adhesion to other extracellular matrix proteins in the airway wall, might also play a similar role. To address this, we performed a screen of integrins expressed on human airway smooth muscle cells using qRT-PCR (Figure 1A and Supplemental Table 1; supplemental material available online with this article; https://doi.org/10.1172/JCI138140DS1). Noting the increased levels of fibronectin, collagens, and laminin chains in asthmatic airways compared with healthy controls (5–8), we identified integrins that regulate adhesion to collagen I and laminin-111. Of the collagen-binding integrins ($\alpha_1\beta_1$, $\alpha_2\beta_1$, $\alpha_{10}\beta_1$, and $\alpha_{11}\beta_1$), integrin $\alpha_{10}\beta_1$ is primarily expressed on chondrocytes, chondrogenic mesenchymal stem cells, endosteum, and periosteum (11–13). We then determined by flow cytometry that integrins $\alpha_1\beta_1$ and $\alpha_2\beta_1$ are expressed on the cell surface of human airway smooth muscle cells but integrin $\alpha_{11}\beta_1$ is not. Of the laminin-binding integrins ($\alpha_3\beta_1$, $\alpha_6\beta_1$, $\alpha_7\beta_1$, and $\alpha_6\beta_4$), integrin $\alpha_6\beta_4$ is primarily expressed on the basal surface of epithelial cells (14). We then determined that integrins $\alpha_3\beta_1$ and $\alpha_6\beta_1$ are expressed on the cell surface of smooth muscle but integrin $\alpha_7\beta_1$ is not (Figure 1B).

To determine the primary integrin(s) responsible for adhesion to collagen I and laminin-111, we performed cell adhesion assays with human airway smooth muscle cells in the presence or absence of specific integrin function-blocking antibodies. Blockade of the α_1 subunit had no effect on adhesion to collagen I, whereas blockade of the α_2 subunit resulted in a dose-dependent decrease in adhesion to collagen I comparable to complete β_1 blockade, suggesting that integrin $\alpha_2\beta_1$ is the principal integrin mediating adhesion of airway smooth muscle cells to collagen I (Figure 2, A and B). Blockade of the α_3 subunit had no effect on adhesion to laminin, whereas blockade of the α_6 subunit resulted in a dose-dependent partial decrease in adhesion to laminin (Figure 2, C and D). Interestingly, although integrin $\alpha_2\beta_1$ is classically defined as a collagen receptor, it has been previously described to also bind laminin (15). We found that blockade of the α_2 subunit resulted in a dose-dependent partial decrease in adhesion of human airway smooth muscle cells to laminin-111, and furthermore that blockade of both integrin subunits α_2 and α_6 reduced adhesion to negligible levels (Figure 2, E and F).

Integrin $\alpha_2\beta_1$ is a potential therapeutic target in the treatment of airway narrowing. To determine the effect of inhibition of integrin $\alpha_2\beta_1$ on contractile responses ex vivo, we measured force genera-

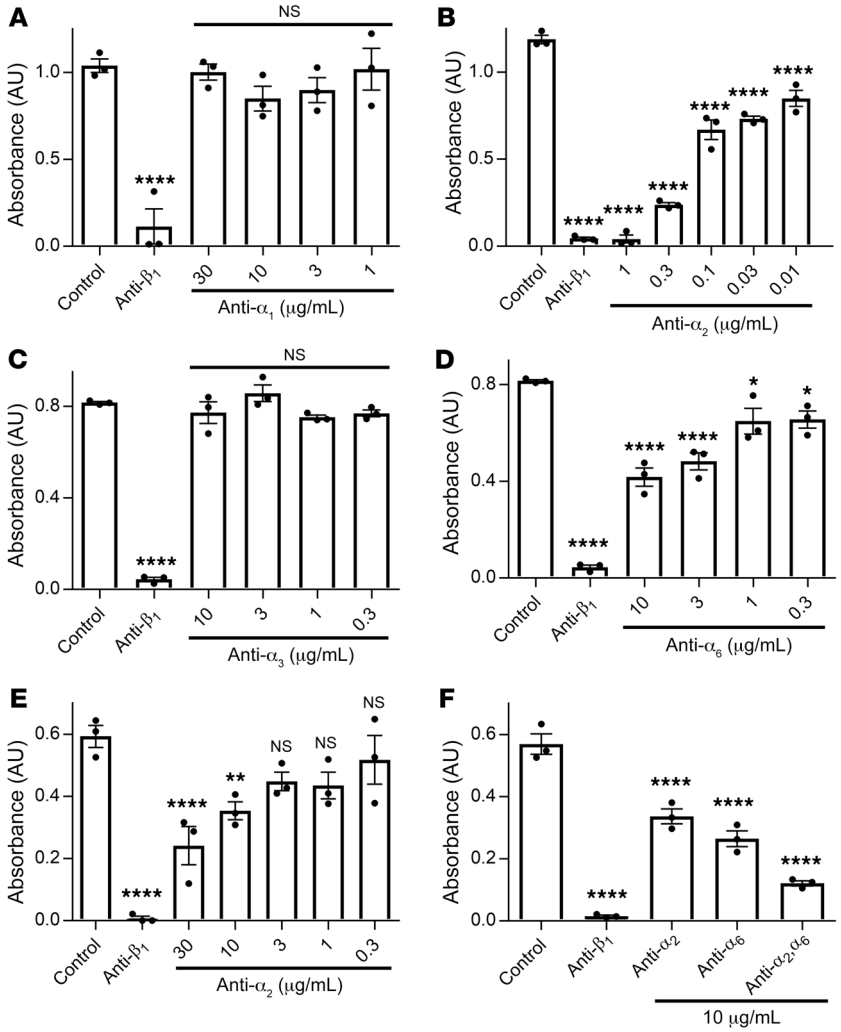

Figure 2. Integrin $\alpha_2\beta_1$ modulates adhesion to collagen I and laminin-111. (**A** and **B**) Adhesion (measured by absorbance of crystal violet at 595 nm) of human airway smooth muscle cells to collagen I (0.1 μg/mL) after treatment with the indicated specific function-blocking integrin antibodies. (**C**–**F**) Adhesion of human airway smooth muscle cells to laminin-111 (5 μg/mL) after treatment with the indicated specific function-blocking integrin antibodies. Experiments performed in triplicate with 3 biological replicates for all panels. $^*P < 0.05$, $^{**}P < 0.01$, $^{****}P < 0.0001$ compared with control; 1-way ANOVA with Dunnett's multiple-comparison test. Data are the mean ± SEM for all panels.

tion in response to increasing concentrations of methacholine in mouse tracheal rings that were treated with IL-13 (or vehicle) for 12 hours and a function-blocking antibody directed against the α_2 subunit (or IgG control). Treatment with the function-blocking antibody had no significant effect on the force generated by rings at baseline but significantly inhibited IL-13–enhanced contraction (Figure 3A). Given the high dose of antibody required to adequately penetrate into tissue, we also tested a small-molecule inhibitor of integrin $\alpha_2\beta_1$ with previously documented in vivo efficacy in a mouse model of arterial thrombosis and renal fibrosis (16, 17). This inhibitor, c15, allosterically regulated integrin $\alpha_2\beta_1$ through interaction with the I-like domain. c15 inhibited human airway smooth muscle cell adhesion to collagen I and laminin-111 in a dose-dependent manner that was similar to the effects of the function-blocking anti-α_2 antibody (Figure 3B). We also showed that c15 did not affect adhesion to other extracellular matrix ligands, such as fibronectin and vitronectin (Supplemental Figure 1). We chose a dose of 10 μg/mL for ex vivo validation, which mimicked the degree of effect of the anti-α_2 function-blocking antibody on collagen I and laminin-111. Treatment with c15 had no significant effect on the force generated by rings at baseline but significantly inhibited IL-13–enhanced contraction in mouse tracheal rings and human bronchial rings (Figure 3, C and D).

To confirm that the effects of c15 were due to blockade of integrin $\alpha_2\beta_1$, we also synthesized a structurally similar c15 methyl ester analog without activity against integrin $\alpha_2\beta_1$ (Supplemental Figure 2A). Treatment with the c15 methyl ester had no significant effect on adhesion of human airway smooth muscle to collagen (Supplemental Figure 2B) and had no protective effect against IL-13–enhanced contraction ex vivo (Supplemental Figure 2C). We also used a structurally distinct inhibitor of the $\alpha_2\beta_1$ I domain, BTT-3033, for ex vivo validation. As expected, treatment with BTT-3033 significantly inhibited IL-13–enhanced contraction (Supplemental Figure 2D).

To determine the effect of inhibition of $\alpha_2\beta_1$ on airway hyperresponsiveness in vivo, we sensitized WT C57BL/6 mice with 3 weekly i.p. injections of OVA followed by 3 consecutive days of i.n. challenge with OVA. On the final day of challenge, we i.p. delivered c15 30 minutes prior to measurement of airway responsiveness to acetylcholine and found that inhibition of $\alpha_2\beta_1$ protected against increased airway hyperresponsiveness after OVA challenge (Figure 3E). Differential counting of cells obtained by bronchoalveolar lavage revealed similar numbers of macrophages, eosinophils, lymphocytes, and neutrophils in the 2 groups (Supplemental Figure 3), suggesting these changes were not due to short-term modulation of the inflammatory response.

One curious aspect of our findings was that the protective effect of c15 occurred only in the setting of exaggerated contraction. To further explore this, we first showed that the protective effect of c15 was preserved in tracheal rings treated with IL-17A, suggesting that the mechanisms responsible for this effect were not cytokine-specific and likely involved a common pathway (Supplemental Figure 4A). We also showed that cell surface expression of integrin $\alpha_2\beta_1$ was not increased after treatment with IL-13 (Supplemental Figure 4B). To determine whether treatment with IL-13 might influence $\alpha_2\beta_1$-mediated adhesion, we compared the ability of human airway smooth muscle cells with or without IL-13 to adhere to varying concentrations of collagen I. Surprisingly, we found that IL-13–treated smooth muscle cells adhered to collagen I better than untreated cells (Figure 4A). We confirmed that this was related to differential effects on integrin activation by demon-

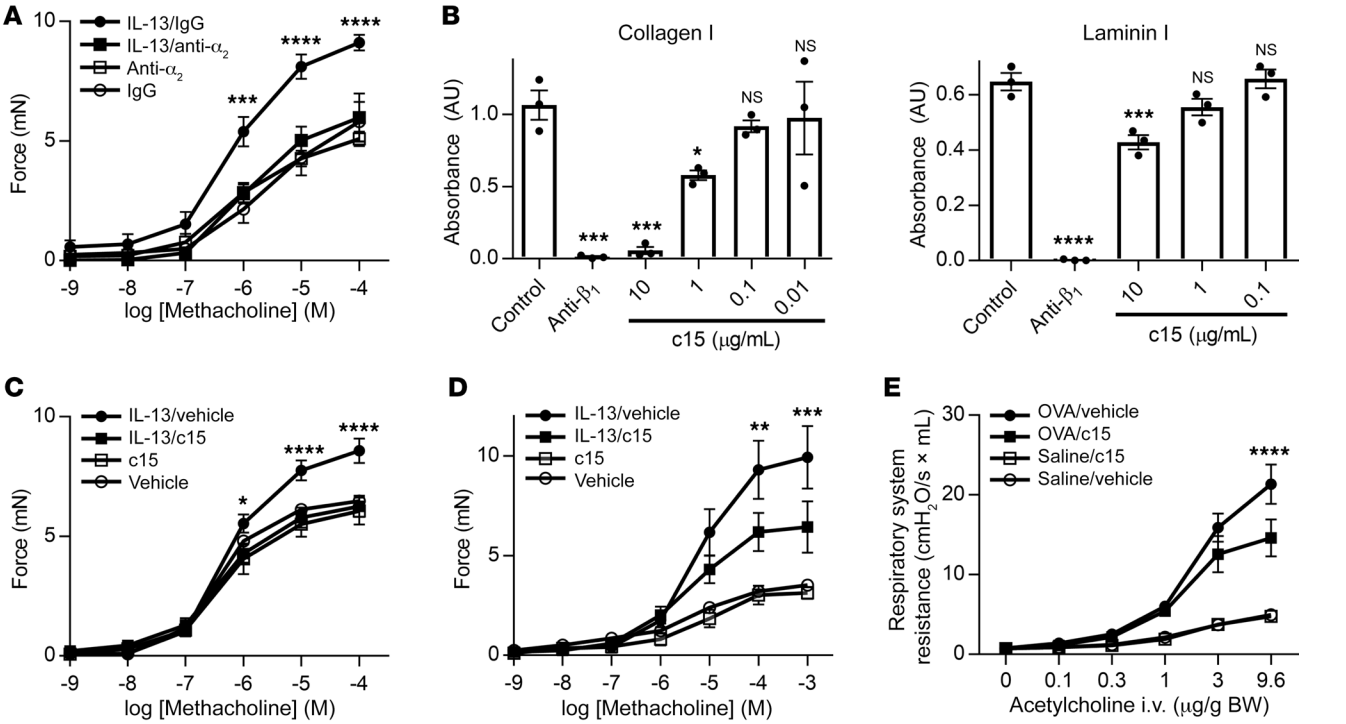

Figure 3. Inhibition of integrin $\alpha_2\beta_1$ protects against cytokine-enhanced contraction. (**A**) Force exerted on mouse tracheal rings measured after incubation for 12 hours with IL-13 (100 ng/mL) or saline, and a function-blocking antibody against integrin α_2 (300 μg/mL) or IgG control with a range of concentrations of methacholine. (**B**) Adhesion (measured by absorbance of crystal violet at 595 nm) of human airway smooth cells to collagen I (0.1 μg/mL) or laminin-111 (5 μg/mL) after treatment with varying concentrations of c15. Experiment performed in triplicate with 3 biological replicates. *$P < 0.05$, ***$P < 0.001$, ****$P < 0.0001$ compared with control; 1-way ANOVA with Dunnett's multiple-comparison test. (**C** and **D**) Force exerted on (**C**) mouse tracheal rings and (**D**) human bronchial rings measured after incubation for 12 hours with IL-13 (100 ng/mL) or saline, and then for 1 hour with c15 (10 μg/mL) or vehicle with a range of concentrations of methacholine. n = 4–7 rings per group for **A**, **C**, and **D**. *$P < 0.05$, **$P < 0.01$, ***$P < 0.001$, ****$P < 0.0001$ between IL-13–treated conditions for **A**, **C**, and **D**. (**E**) Respiratory system resistance in WT C57Bl/6 mice after immunization and i.n. challenge with OVA, with i.p. administration of c15 (120 mg/kg) or vehicle (50% DMSO, 0.9% saline) 30 minutes prior to measurements. n = 9–10 animals per group. ****$P < 0.0001$ between OVA treated conditions; 2-way ANOVA with repeated measures, Tukey's multiple-comparison test for **A** and **C**–**E**. Data are the mean ± SEM for all panels.

strating that treatment with IL-13 resulted in increased activated β_1 integrin at the cell surface as detected by an antibody that recognized an activation-dependent epitope (Figure 4B).

To further elucidate whether c15 acts on integrin $\alpha_2\beta_1$ from the smooth muscle or epithelium, we denuded the epithelium from tracheal rings and measured the effect of c15 on IL-13–enhanced contraction (Supplemental Figure 5A). As reported by others, epithelial removal enhanced the amount of force generation in response to methacholine (Supplemental Figure 5B) (18, 19). In tracheal rings denuded of epithelium, c15 protected against IL-13–enhanced contraction to a similar degree as intact tracheal rings, suggesting that c15 acted directly on smooth muscle (Supplemental Figure 5C).

Integrin $\alpha_2\beta_1$ mitigates airway narrowing without affecting smooth muscle shortening. Force generation in airway smooth muscle depends on activation of the actin-myosin power stroke and firm adhesion of muscle to the surrounding extracellular matrix. We have already shown that inhibition of integrin $\alpha_5\beta_1$–mediated tethering to extracellular fibronectin can alter exaggerated force generation without affecting calcium homeostasis or phosphorylation of myosin light chain or its regulatory proteins (10). We therefore determined the effect of inhibition of integrin $\alpha_2\beta_1$ on phosphorylation of myosin light chain. As expected, IL-13 increased myosin light chain phosphorylation in response to methacholine, but inhibition of integrin $\alpha_2\beta_1$ did not modulate this effect. Total myosin light chain levels were not significantly altered either by treatment with IL-13 or by the addition of c15 (Figure 4C).

Our previous work suggested that integrin inhibition reduced force transmission by reducing the tethering of airway smooth muscle to the surrounding tissue. To more directly evaluate whether the reductions in force generation we observed were mainly explained by decreased tethering of contracting airway smooth muscle, we developed a method to simultaneously quantify airway narrowing and smooth muscle shortening in intact tracheas using 2-photon laser scanning microscopy (hereafter referred to as 2-photon microscopy). We reasoned that a loss of tethering should reduce the degree of airway narrowing while leaving smooth muscle shortening largely intact, whereas any effect on smooth muscle contractility should lead to proportionate reductions in shortening and narrowing. We dissected tracheal rings from mice with red fluorescent protein (RFP) expressed under the control of an α-smooth muscle actin (α-SMA) promoter. These rings were mounted onto coverslips with the ventral side down, so that the smooth muscle–rich dorsal portion of the trachea was unrestricted. The trachea was then imaged in cross-section to capture the signal from RFP, and second harmonic generation was used to visualize surrounding collagen fibers. Tissue autofluorescence aided in the measure-

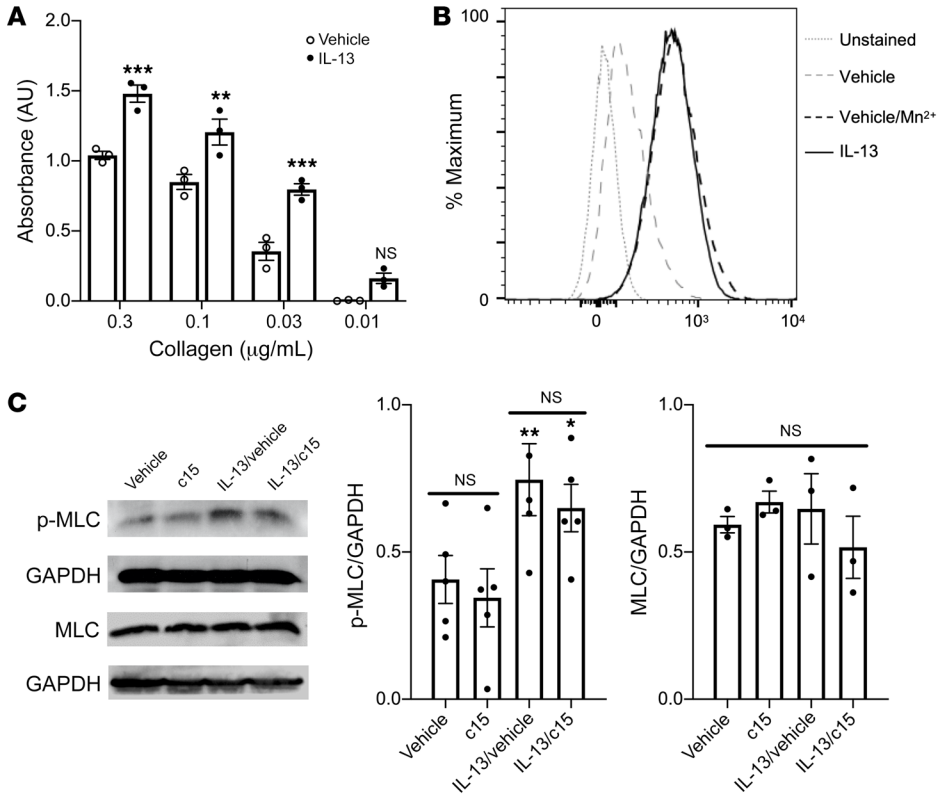

Figure 4. IL-13 activates β_1 integrins to promote adhesion without altering intracellular signaling. (**A**) Adhesion (measured by absorbance of crystal violet at 595 nm) of human airway smooth muscle cells to the indicated concentrations of collagen I after incubation for 12 hours with IL-13 (100 ng/mL) or saline. NS = not significant, $^{**}P < 0.01$, $^{***}P < 0.001$ compared with vehicle; 2-way ANOVA with Tukey's multiple-comparison test. Experiment performed in triplicate with 3 biological replicates. (**B**) Human airway smooth muscle cells were incubated for 12 hours with IL-13 (100 ng/mL), 20 minutes with Mn^{2+} (1 mM), or saline, then suspended and labeled with a primary antibody specific for activated integrin β_1 and a secondary antibody conjugated to allophycocyanin (APC). Cells were then analyzed by flow cytometry and gated for live cells. The resultant population was analyzed for APC expression. Human airway smooth muscle cells labeled with secondary antibody alone served as an unstained control (gray short dashed line). Vehicle is shown by a long, gray dashed line. Vehicle/Mn^{2+} is shown by a long, black dashed line. IL-13 is shown by a solid black line. Representative histogram of APC expression (MFI) versus cell count scaled to mode (percentage of maximum) is shown. Results verified with 2 biological replicates. (**C**) Representative Western blot of phosphorylation of myosin light chain (p-MLC) and total myosin light chain (MLC) after incubation for 12 hours with IL-13 (100 ng/mL) or saline, and then for 1 hour with c15 (10 μg/mL) or vehicle followed by a single dose of methacholine (10^{-4} M). GAPDH used as a loading control. Densitometric data are from n = 3–5 independent experiments. $^{*}P < 0.05$, $^{**}P < 0.01$ compared with vehicle; 2-way ANOVA with Tukey's multiple-comparison test. Data are the mean ± SEM for all panels.

ment of the cross-sectional area of the trachea. Images were taken at baseline and after treatment with methacholine under various conditions (Figure 5A and Supplemental Videos 1 and 2). In order to ensure there were no systematic differences across groups, we verified that the ratio of tracheal smooth muscle length to ring circumference at baseline was not significantly different between groups at baseline (Supplemental Figure 6A).

To determine the degree of airway narrowing, we measured the cross-sectional area of the trachea using ImageJ (NIH). As expected, treatment with methacholine caused narrowing of the tracheal lumen compared with baseline; exposure to c15 did not significantly alter this response. Treatment with IL-13 enhanced airway narrowing, and treatment with c15 inhibited IL-13–enhanced airway narrowing, consistent with our in vivo results. Similarly, treatment with an inhibitor of Rho-associated protein kinase, Y-27632, a classic inhibitor of airway smooth muscle contraction, inhibited the IL-13–induced enhancement of airway narrowing (Figure 5B).

For simultaneous measurement of muscle shortening, we rotated the image of the tracheal ring in Imaris to obtain a coronal view (Supplemental Videos 1 and 2). Given the variability in the length of individual smooth muscle fibers comprising the posterior trachea and the difficulty of tracking the same fiber between images, we calculated the area and volume encompassed by the RFP signal representing smooth muscle in 2 and 3 dimensions, respectively. As expected, we found that methacholine caused the muscle to shorten and the smooth muscle area and volume to decrease compared with baseline conditions, as has been described by others (20). This effect was not significantly altered after treatment with c15. Treatment with IL-13 enhanced muscle shortening and led to a marked decrease in smooth muscle area and volume. However, when IL-13–treated tracheas were incubated with c15, the muscle shortening was unchanged compared with IL-13 treatment alone. In contrast, when IL-13–treated tracheas were incubated with Y-27632, muscle shortening was impaired after treatment with methacholine, reflecting inhibition of the core actin-myosin machinery (Figure 5C).

To further validate our hypothesis that blockade of integrin $\alpha_2\beta_1$ affects tethering of smooth muscle to adjacent collagen, we used 2-photon microscopy to quantify changes in cellular tethering. Although changes in tethering occur around individual smooth muscle cells within the muscle strip and at the border between smooth muscle and adjacent cartilage rings, we focused on the latter because of the ease of visually distinguishing the RFP signal of smooth muscle from adjacent structures and the ability to leverage intrinsic tissue features of cartilage that could be used as fiducial markers. We imaged the dorsal portion of the trachea in a coronal plane and selected intrinsic fiducial markers within the cartilage that were along the vector of the muscle fiber and within 100 μm of the edge of smooth muscle to measure changes in distance. Treatment with methacholine resulted in an increase in the distance between the smooth muscle edge and the fiducial marker, an effect not significantly changed after exposure to either c15 or IL-13

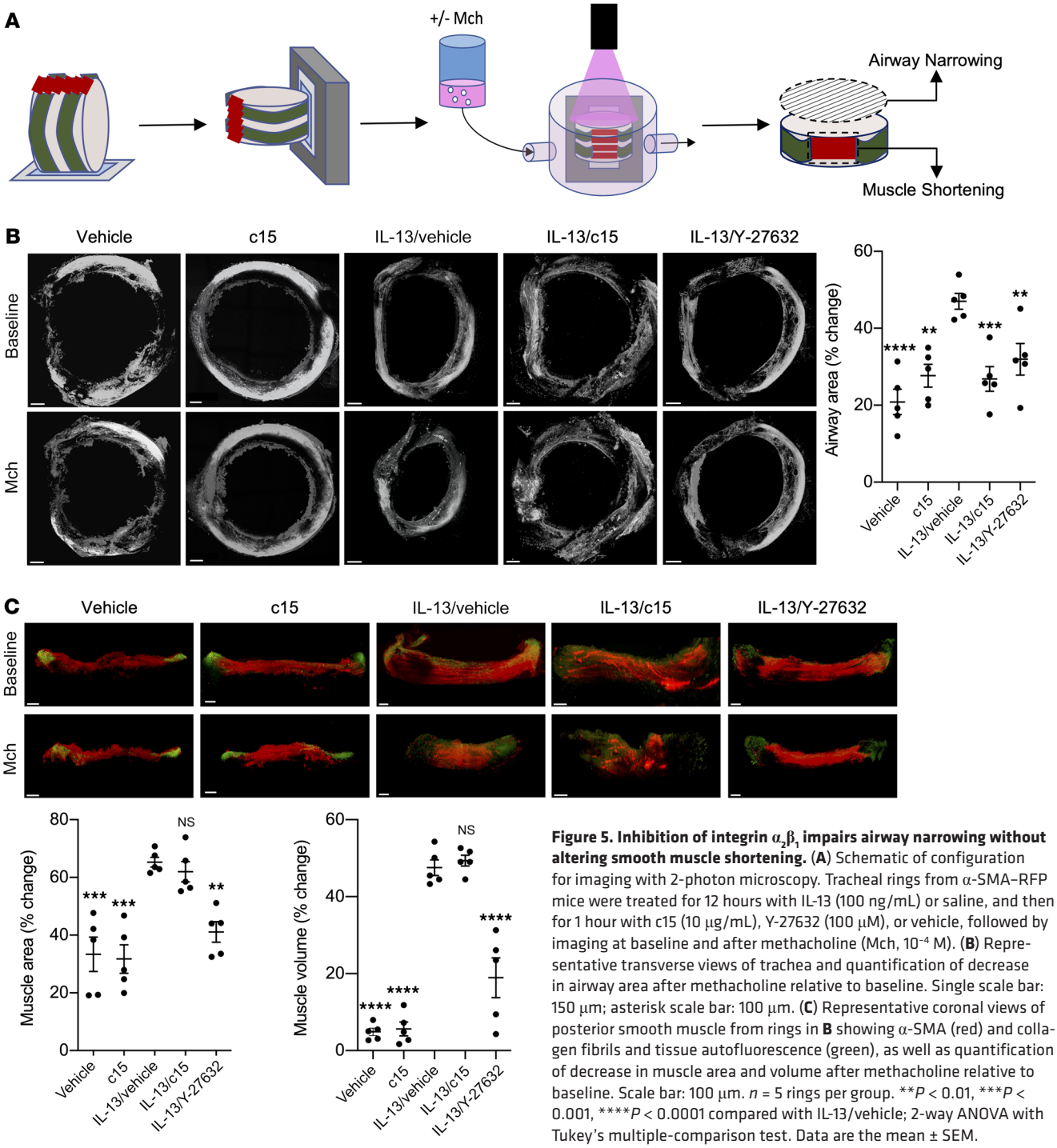

Figure 5. Inhibition of integrin $\alpha_2\beta_1$ impairs airway narrowing without altering smooth muscle shortening. (**A**) Schematic of configuration for imaging with 2-photon microscopy. Tracheal rings from α-SMA–RFP mice were treated for 12 hours with IL-13 (100 ng/mL) or saline, and then for 1 hour with c15 (10 μg/mL), Y-27632 (100 μM), or vehicle, followed by imaging at baseline and after methacholine (Mch, 10^{-4} M). (**B**) Representative transverse views of trachea and quantification of decrease in airway area after methacholine relative to baseline. Single scale bar: 150 μm; asterisk scale bar: 100 μm. (**C**) Representative coronal views of posterior smooth muscle from rings in **B** showing α-SMA (red) and collagen fibrils and tissue autofluorescence (green), as well as quantification of decrease in muscle area and volume after methacholine relative to baseline. Scale bar: 100 μm. n = 5 rings per group. $^{**}P < 0.01$, $^{***}P < 0.001$, $^{****}P < 0.0001$ compared with IL-13/vehicle; 2-way ANOVA with Tukey's multiple-comparison test. Data are the mean ± SEM.

alone. However, when IL-13–treated rings were exposed to c15, the distance between the smooth muscle edge and the fiducial marker increased further, reflecting the loss of cellular tethering of muscle to the surrounding matrix (Figure 6, A and B). We also confirmed that treatment with c15, IL-13, or both did not change the distance between individual fiducial markers extrinsic to airway smooth muscle, suggesting that this effect was specific to the tethering of muscle to the surrounding matrix (Supplemental Figure 6B).

Taken together, these data confirmed that blockade of integrin $\alpha_2\beta_1$ inhibited cytokine-enhanced airway narrowing without significant alteration of smooth muscle shortening in a manner consistent with loss of tethering and quite distinct from conventional inhibitors of smooth muscle contraction.

Discussion

In the present study, we demonstrated that blockade of integrin $\alpha_2\beta_1$ protected against exaggerated force generation induced by a disease-relevant cytokine in airway smooth muscle. Notably, our mechanistic studies suggest that these effects did not occur through modulation of actin-myosin cross-bridge interactions, but

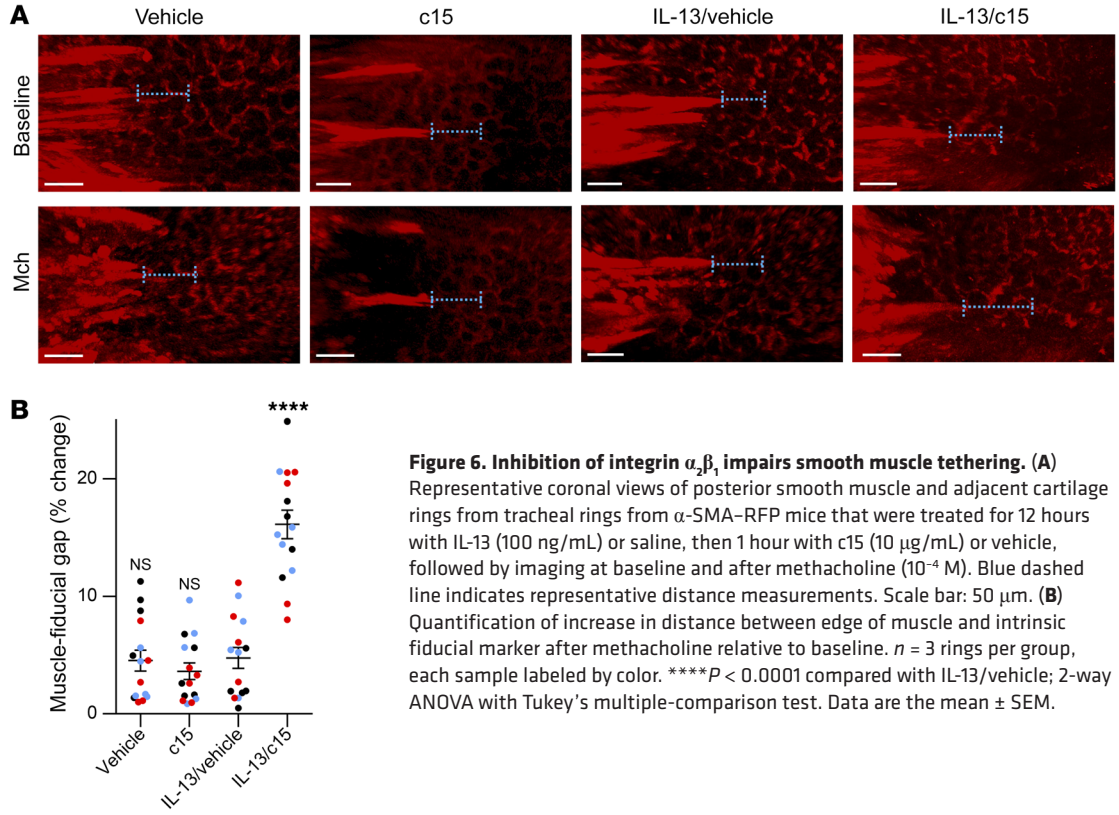

Figure 6. Inhibition of integrin $\alpha_2\beta_1$ impairs smooth muscle tethering. (**A**) Representative coronal views of posterior smooth muscle and adjacent cartilage rings from tracheal rings from α-SMA–RFP mice that were treated for 12 hours with IL-13 (100 ng/mL) or saline, then 1 hour with c15 (10 μg/mL) or vehicle, followed by imaging at baseline and after methacholine (10^{-4} M). Blue dashed line indicates representative distance measurements. Scale bar: 50 μm. (**B**) Quantification of increase in distance between edge of muscle and intrinsic fiducial marker after methacholine relative to baseline. n = 3 rings per group, each sample labeled by color. ****$P < 0.0001$ compared with IL-13/vehicle; 2-way ANOVA with Tukey's multiple-comparison test. Data are the mean ± SEM.

rather by modulating cellular tethering to the extracellular matrix. Members of the integrin family have previously been described to have effects on airway hyperresponsiveness (21, 22) by modulating intracellular pathways resulting in downstream regulation of myosin light chain phosphorylation, including interaction with SSAT and PTEN. However, there is a growing body of evidence supporting the role of independently regulated cellular processes, including cytoskeletal stabilization (23, 24), matrix stiffness (25, 26), and intercellular tethering (27, 28), in modulating force transmission throughout smooth muscle bundles.

Our group has previously shown that mouse mast cell protease 4 and its human orthologue chymase can inhibit IL-13–induced enhancement of force transmission by murine and human airway rings through cleavage of the extracellular matrix protein fibronectin (10, 29). We further showed that inhibition of the $\alpha_5\beta_1$ integrin, the major fibronectin receptor on airway smooth muscle, is as effective in inhibiting IL-13–induced enhancement of force transmission as chymase. These findings led us to hypothesize that inhibition of integrin-mediated airway smooth muscle tethering could be a novel strategy for treating asthma and other diseases characterized by exaggerated airway narrowing.

Our hypothesis led us to generate 2 testable predictions: (1) other extracellular matrix ligands may participate in integrin-mediated force transmission, and (2) inhibitors of these tethering pathways should inhibit airway narrowing without altering smooth muscle shortening. The data presented in this paper supported both of these predictions. Specifically, we identified that integrin $\alpha_2\beta_1$ binds to 2 extracellular matrix ligands distinct from integrin $\alpha_5\beta_1$, and this integrin can be targeted to abrogate IL-13–enhanced contraction. In addition, we directly demonstrated with 2-photon microscopy that inhibition of this integrin modulated smooth muscle tethering to impede airway narrowing without altering smooth muscle shortening. Taken together, the data presented in this paper provide strong support for the idea that smooth muscle–mediated airway narrowing can be inhibited by directly interfering with integrin-mediated smooth muscle tethering, and notably this can be done without inhibition of actin/myosin-mediated contraction.

One interesting aspect of our findings is that all our interventions targeting integrin $\alpha_2\beta_1$ did not affect baseline contraction but had measurable effects only in the setting of pretreatment with asthmagenic cytokines or allergen sensitization and challenge. There are several examples in the literature of differential effects being observed in the setting of an allergic environment, including loss of integrin β_6 (29), inhibition of integrin α_5 (10), and loss of milk fat globule–epidermal growth factor–factor VIII (30). We interpret our results to be consistent with the hypothesis that under normal conditions, there is enough redundancy in cell-matrix interactions that loss of an individual tether would not be sufficient to prevent contracting muscle from generating force. Our observation that IL-13 influenced the activation state of β_1 integrins and promoted adhesion of integrin $\alpha_2\beta_1$ to its ligand collagen I lends traction to the idea that under pathological conditions simulated by cytokines and allergen exposure, multiple cell-matrix tethering pathways are maximally engaged. In this context, it would not be surprising that disruption of a single tethering pathway has more substantial effects on the ability to sustain exaggerated force.

In these studies, we identified integrin $\alpha_2\beta_1$ as the major adhesion receptor for collagen I and an important adhesion receptor for laminin-111 on human airway smooth muscle. The most frequently studied ligand of integrin $\alpha_2\beta_1$ is collagen, which it binds with high affinity by recognizing the GFOGER sequence in the collagen triple helix (31). However, integrin $\alpha_2\beta_1$ has also been described to mediate binding to laminin isoforms in a manner that is incompletely understood and thought to be cell-type specific (15, 32). Our findings that integrin $\alpha_2\beta_1$ can partially inhibit the ability of human airway smooth muscle cells to bind to laminin is consistent with these observations about integrin-ligand promiscuity, and in our mind makes integrin $\alpha_2\beta_1$ a particularly attractive therapeutic target because it is capable of regulating adhesion to 2 matrix proteins that are present in high concentration surrounding airway smooth muscle.

Our application of 2-photon microscopy to simultaneously visualize airway narrowing and directly quantify muscle shortening is, we believe, a powerful tool to directly evaluate the relationship between smooth muscle shortening and airway narrowing in live tissue. Although various imaging methods can be used to estimate muscle shortening and force transmission in live cells (33), these methods do not reflect the complexity of the heterogeneous structures of the airways. In tissue, force generation has been quantified by ex vivo perfusion in a muscle bath, but this method has not generally allowed simultaneous quantification of muscle shortening. Our method allows for concurrent assessment of both parameters in the same tissue sample. Our finding that blockade of integrin $\alpha_2\beta_1$ led to a reduction in exaggerated airway narrowing without altering smooth muscle shortening depends on this simultaneous assessment, and when paired with concurrent quantification of changes in stretch between muscle and matrix, this finding underscores the importance of cellular tethering in effective transmission of force by contracting airway smooth muscle.

Significant strides have been made in understanding the effects of IL-13, IL-17A, and other cytokines in regulating the varied immune response in asthma (34–38), but most of these therapeutic targets have met with limited success in only a small subset of patients with asthma in clinical trials (39–43). In contrast, despite the critical importance of airway smooth muscle in the pathophysiology of asthma and its contribution to bronchospasm, there has been little progress in defining novel pathways targeting airway smooth muscle in the last several decades (44). Our demonstration that inhibition of integrin-mediated airway smooth muscle tethering can inhibit pathological force generation in smooth muscle through a mechanism independent of conventional bronchodilator therapy identifies an exciting opportunity for the development of new treatments for diseases characterized by exaggerated airway narrowing. Inhibitors of integrin $\alpha_2\beta_1$ have been administered to humans in numerous clinical trials targeting multiple sclerosis (45), inflammatory bowel disease (46), and cancer (47) and are generally well tolerated; the only side effect is minimal inhibition of platelet adhesion (less than that caused by low-dose aspirin) (48, 49). These results suggest that toxicity is not likely to be an impediment to the development of potent $\alpha_2\beta_1$ inhibitors that can be accelerated into clinical trials for asthma.

In summary, we found that blockade of integrin $\alpha_2\beta_1$ inhibited pathological force generation by airway smooth muscle by inhibiting the adhesion to extracellular collagen I and laminin-111. Mechanistically, this effect occurred without affecting actin myosin contraction or airway smooth muscle shortening, implying that cellular tethering is a powerful mediator of airway narrowing in muscle. These findings identified integrin $\alpha_2\beta_1$ as a therapeutic target in asthma.

Methods

Reagents. Rabbit Ser19 phospho-myosin light chain (3671), myosin light chain (8505), and GAPDH antibodies were purchased from Cell Signaling Technology. c15 and BTT-3033 were purchased from Tocris. Y-27632 was purchased from Sigma-Aldrich. Integrin antibodies used were monoclonal anti–integrin α_1 (FB12, MilliporeSigma), α_2 (P1E6, MilliporeSigma and HMa2, Invitrogen), α_3 (P1B5, BioLegend), α_6 (NKI-GoH3, MilliporeSigma), α_7 (6A11, MBL) (50, 51), α_{11} (203E3, a gift from Donald Gullberg at the University of Bergen, Norway) (52), and activated β_1 (HUTS-4, MilliporeSigma). Monoclonal anti–integrin α_v (L230) and β_1 (P5D2) were purified in our lab from a hybridoma obtained from ATCC and DSHB, respectively. c15 methyl ester was synthesized in our laboratory.

Cells. Human airway smooth muscle cells and media were purchased from Lonza and cultured according to the vendor's instructions. Cells were used between passage 5 and 10.

Mice. Mice used for all experiments were in a C57BL/6 background, 6–10 weeks old, and housed under specific pathogen–free conditions in the Animal Barrier Facility at UCSF. WT mice were purchased from The Jackson Laboratory. α-SMA–RFP mice were obtained from David Brenner at UCSD (53). Sex-matched littermate controls were used in all experiments for tracheal ring contractility and airway hyperresponsiveness.

Murine models of allergic airway disease. Assessment of airway hyperresponsiveness was performed as described previously (21, 54). Briefly, 7-week-old sex-matched C57/Bl6 mice were sensitized on days 0, 7, and 14 by i.p. injection of 50 μg OVA emulsified in 1 mg of aluminum potassium sulfate. Subsequently, mice were anesthetized with isoflurane and i.n. challenged on 3 consecutive days (days 21, 22, and 23) by aspiration of 100 μg OVA dissolved in 40 μL saline. Twenty-four hours after the last challenge, mice were anesthetized with isoflurane and underwent computer-generated randomization to be i.p. administered either c15 (120 mg/kg in 50% DMSO, 0.9% sodium chloride) or vehicle (50% DMSO, 0.9% sodium chloride). Then, 30 minutes after administration, mice were anesthetized with ketamine (100 mg/kg), xylazine (10 mg/kg), and acepromazine (3 mg/kg). Respiratory system resistance was determined using invasive cannulation of the trachea. Scientists were blinded to the drug delivered throughout the experiment and during analysis of the experimental outcome.

Assessment of pulmonary inflammation and mucus production. Lungs were subjected to 5 consecutive lavages with 0.8 mL of PBS. After lysing red blood cells, the total cells were counted with a hemocytometer. Cytospin preparations were stained with a HEMA 3-stain set (Thermo Fisher Scientific), and cell differential percentages were determined based on light microscopic evaluation of greater than 300 cells per slide. Lavaged lungs were inflated with 10% buffered formalin to 25 cm H_20 of pressure. Multiple paraffin-embedded 5-μm sections of the entire mouse lung were prepared and stained with H&E and periodic acid–Schiff (PAS) to evaluate mucus production.

Measurement of tracheal smooth muscle contractility. Tracheal ring contraction studies were performed as described previously (21, 54).

Briefly, after incubation with the indicated inhibitor, rings were equilibrated under 0.5 gm of applied tension, contracted with 60 mM KCl, and only rings that generated more than 1 mN of force were analyzed. After reequilibration, contractile responses were evaluated to increasing doses of methacholine (Sigma-Aldrich). For analysis of suppressive effects on cytokine-induced contractility, rings were treated with human IL-13 (100 ng/mL; Peprotech) or human IL-17A (100 ng/mL; Peprotech) for 12 hours at 37°C with 5% CO_2. For epithelial debridement experiments, we removed the epithelium by gentle rubbing with a PE-10 tube polished with 60-grit sandpaper (29). Epithelial removal was confirmed by microscopic observation of H&E-stained sections of at least 3 rings per group. For human bronchial rings, lung tissue was obtained from lung transplant donors. Bronchi, 5–8 mm in diameter, were dissected free of connective tissue and cut into 4 mm thick rings. Rings were stored and assessed as above, except a resting tension of 1*g* was applied, and rings were first contracted with 120 mM KCl after equilibration for 2 hours, and only the rings that generated more than 2 mN of force were used for experiments.

Immunoblots. Smooth muscle dissected from mouse tracheas were homogenized in lysis buffer (50 mM Tris-HCl, pH 7.5, 10 mM $MgCl_2$, 150 mM NaCl, 1% Triton X-100, 10 mM NaF, 1 mM Na_3VO_4) with protease and phosphatase inhibitor cocktail (Thermo Fisher Scientific). Lysates were centrifuged, and the supernatant was resolved by SDS-PAGE and transferred to a PVDF membrane (MilliporeSigma). Membranes were blocked for 1 hour with 5% BSA in Tris-buffered saline with Tween-20, incubated at room temperature for 2 hours with primary antibodies, washed in Tris-buffered saline with Tween-20, incubated for 1 hour with peroxidase-conjugated secondary antibody, washed in Tris-buffered saline with Tween-20, and developed with ECL plus (PerkinElmer) prior to chemiluminescence detection (Bio-Rad Laboratories). All quantitative densitometry was calculated with ImageJ (NIH).

Flow cytometry. Human airway smooth muscle cells were harvested with 0.25% trypsin-EDTA, washed twice with PBS, and resuspended in FACS buffer (PBS supplemented with 10% serum and 1% BSA). Then, 5×10^5 cells were incubated with a primary antibody at 4°C for 30 minutes in the dark. Cells were then washed, resuspended in FACS buffer, and incubated with secondary goat anti-mouse antibody conjugated to allophycocyanin (APC) (Jackson ImmunoResearch) or goat anti-rat antibody conjugated to FITC (Jackson ImmunoResearch). Cells were then washed, resuspended in 2.5% serum, and analyzed on a BD Biosciences FACSCanto II. Antibodies were used at 10 μg/mL. For experiments studying integrin activation, all solutions were prepared in HEPES-buffered saline without calcium and magnesium. Integrin activation was achieved with exposure to Mn^{2+} (1 mM) for 20 minutes before incubating with primary antibody.

qRT-PCR. Total RNA was isolated with the RNeasy kit (QIAGEN). cDNA was analyzed by SYBR-Green real-time PCR with an ABI 7900HT thermocycler and normalized to GAPDH expression.

Cell adhesion assay. First, 96-well flat-bottomed tissue culture plates (Linbro) were coated with 0.1 μg/mL rat tail collagen I (MilliporeSigma), 5 μg/mL laminin-111 (R&D Systems), 5 μg/mL fibronectin (MilliporeSigma), or 5 μg/mL vitronectin (R&D Systems) for 1 hour at 37°C. After incubation, wells were washed with PBS, then blocked with 1% BSA at 37°C for 1 hour. Control wells were filled with 1% BSA. Human airway smooth muscle cells were detached using 10 mM EDTA and resuspended in serum-free DMEM. For blocking experiments, cells were incubated with the indicated concentration of antibody or compound for 15 minutes at 4°C before plating. The plates were centrifuged at 10*g* for 5 minutes before incubation for 1 hour at 37°C in humidified 5% CO_2. Nonadherent cells were removed by centrifugation (top side down) at 10*g* for 5 minutes. Attached cells were stained with 0.5% crystal violet and the wells were washed with PBS. The relative number of cells in each well was evaluated after solubilization in 40 μL of 2% Triton X-100 by measuring absorbance at 595 nm in a microplate reader (Bio-Rad Laboratories). All determinations were carried out in triplicate.

Two-photon microscopy. Tracheal rings dissected from α-SMA–RFP mice were attached to a 1 mm × 3 mm plastic coverslip using tissue adhesive glue (3M, Vetbond). Samples were stored overnight at 37°C in 5% CO_2 in serum-free DMEM with pen-strep. The coverslip was then mounted on a metal plate so the tracheal ring could be placed in a heated chamber (JG-23W/HP, Warner Instruments) attached to a PM-1 chamber platform and a Series 20 stage adapter using a small amount of silicone vacuum grease (Beckman Coulter). DMEM that was warmed by an in-line heater (Warner Instruments) was passed through the sample at a rate of 1.5 mL/min. Media temperature in the imaging chamber was maintained at 35°C–37°C with a dual temperature controller (Warner Instruments). Carbogen (5% CO_2/95% O_2) was bubbled into the DMEM to maintain physiological pH. Methacholine was added at a concentration of 10^{-4} M for analysis of contractile response. Tracheal explants were imaged on an LSM 7 MP INDIMO 2-photon microscope (Carl Zeiss Microscopy) equipped with a Chameleon Ultra II laser (Coherent) and a Compact Optical Parametric Oscillator (Coherent) and a W Plan-Apochromat 20×/1.0 objective. Images were collected on non-descanned gallium arsenide phosphide (GaAsP) detectors. The Chameleon laser, which pumps the OPO, was tuned to 860–870 nm and was used to excite tissue autofluorescence and for second harmonic generation. The OPO was tuned to 1100–1120 nm to excite RFP that was detected using a 605/70 bandpass filter (ET605/70 m, Chroma). Collagen bands, visualized by second harmonic generation, were detected using a 450 short-pass filter (HQ450SP-2P, Chroma). Tissue autofluorescence was visualized in the above channels or in a 525/50 bandpass filter (ET525/50 m, Chroma). Image analysis was done using Imaris software (Bitplane) and ImageJ. For volume rendering, 3D reconstruction of the smooth muscle was generated using the surface feature on Imaris. For fiducial distances, only intrinsic fiducials that were clearly identifiable before and after contraction were used. For measurements that involved muscle, fiducials that were within 100 μm of the edge of muscle and aligned with the vector of the muscle fiber were chosen for subsequent analysis in Imaris. Scientists were blinded to the drug delivered during analysis of the experimental outcome.

Statistics. The statistical significance of the differences within or between multiple groups was calculated with 1-way or 2-way ANOVA with repeated measures of variance for related samples, and when differences were statistically significant ($P \leq 0.05$), this was followed by a Dunnett's or Tukey's *t* test for subsequent pairwise analysis. All calculations were performed using Prism (GraphPad Software).

Study approval. All mice were housed in a specific pathogen–free animal facility at UCSF. All animal studies were approved by the IACUC at UCSF in accordance with NIH guidelines. For human bronchial contractility experiments, cadaveric human lungs were obtained

from brain-dead donors whose lungs could not be used for transplantation and therefore did not require approval of the UCSF Committee on Human Research.

Author contributions

AS designed the research studies and prepared the manuscript. XT, CA, and DS provided revisions to the manuscript. SL, UN, XT, XR, WQ, and AS performed the experiments. SL, UN, XR, and AS collected and analyzed the data. XH, WD, CA, HJ, and DS provided reagents, equipment, and conceptual advice.

Acknowledgments

We thank the late Xiaozhu Huang for her invaluable technical advice. This work was supported by grants from the National Heart, Lung, and Blood Institute (NHLBI), NIH (K08HL124049) and the UCSF Nina Ireland Program for Lung Health (to AS); the National Institute of Allergy and Infectious Diseases (NIAID), NIH (U19AI077439, to DS); the NHLBI (DP2HL117752) and the Program for Breakthrough Biomedical Research, which is partially funded by the Sandler Foundation (to CDCA); the National Human Genome Research Institute, NIH (R35GM122603, to WD); and the University of California Center for Accelerated Innovation/NHLBI (U54HL119893, to DS and WD).

Address correspondence to: Aparna B. Sundaram, University of California, San Francisco, 513 Parnassus Avenue, Box 0130, San Francisco, California 94143, USA. Phone: 415.514.8363; Email: aparna.sundaram@ucsf.edu.

1. Bousquet J, et al. Asthma. From bronchoconstriction to airways inflammation and remodeling. *Am J Respir Crit Care Med*. 2000;161(5):1720–1745.
2. Davies DE, et al. Airway remodeling in asthma: new insights. *J Allergy Clin Immunol*. 2003;111(2):215–225.
3. Postma DS, Kerstjens HA. Characteristics of airway hyperresponsiveness in asthma and chronic obstructive pulmonary disease. *Am J Respir Crit Care Med*. 1998;158(5 pt 3):S187–S192.
4. Dekkers BGJ, et al. Airway structural components drive airway smooth muscle remodeling in asthma. *Proc Am Thorac Soc*. 2009;6(8):683–692.
5. Roche WR, et al. Subepithelial fibrosis in the bronchi of asthmatics. *Lancet*. 1989;1(8637):520–524.
6. Amin K, et al. Uncoordinated production of Laminin-5 chains in airways epithelium of allergic asthmatics. *Respir Res*. 2005;6:110.
7. Altraja A, et al. Expression of laminins in the airways in various types of asthmatic patients: a morphometric study. *Am J Respir Cell Mol Biol*. 1996;15(4):482–488.
8. Tran T, et al. Endogenous laminin is required for human airway smooth muscle cell maturation. *Respir Res*. 2006;7(1):117.
9. Sun Z, et al. Extracellular matrix-specific focal adhesions in vascular smooth muscle produce mechanically active adhesion sites. *Am J Physiol Cell Physiol*. 2008;295(1):C268–C278.
10. Sundaram A, et al. Targeting integrin α5β1 ameliorates severe airway hyperresponsiveness in experimental asthma. *J Clin Invest*. 2017;127(1):365–374.
11. Camper L, et al. Distribution of the collagen-binding integrin alpha10beta1 during mouse development. *Cell Tissue Res*. 2001;306(1):107–116.
12. Camper L, et al. Isolation, cloning, and sequence analysis of the integrin subunit alpha10, a beta1-associated collagen binding integrin expressed on chondrocytes. *J Biol Chem*. 1998;273(32):20383–20389.
13. Varas L, et al. Alpha10 integrin expression is up-regulated on fibroblast growth factor-2-treated mesenchymal stem cells with improved chondrogenic differentiation potential. *Stem Cells Dev*. 2007;16(6):965–978.
14. Stepp MA, et al. Alpha 6 beta 4 integrin heterodimer is a component of hemidesmosomes. *Proc Natl Acad Sci U S A*. 1990;87(22):8970–8974.
15. Languino LR, et al. Endothelial cells use alpha 2 beta 1 integrin as a laminin receptor. *J Cell Biol*. 1989;109(5):2455–2462.
16. Miller MW, et al. Small-molecule inhibitors of integrin alpha2beta1 that prevent pathological thrombus formation via an allosteric mechanism. *Proc Natl Acad Sci U S A*. 2009;106(3):719–724.
17. Borza CM, et al. Inhibition of integrin α2β1 ameliorates glomerular injury. *J Am Soc Nephrol*. 2012;23(6):1027–1038.
18. Barnes PJ, et al. The effect of airway epithelium on smooth muscle contractility in bovine trachea. *Br J Pharmacol*. 1985;86(3):685–691.
19. Barnett K, et al. The effects of epithelial cell supernatant on contractions of isolated canine tracheal smooth muscle. *Am Rev Respir Dis*. 1988;138(4):780–783.
20. Fay FS, Delise CM. Contraction of isolated smooth-muscle cells--structural changes. *Proc Natl Acad Sci U S A*. 1973;70(3):641–645.
21. Chen C, et al. Integrin α9β1 in airway smooth muscle suppresses exaggerated airway narrowing. *J Clin Invest*. 2012;122(8):2916–2927.
22. Khalifeh-Soltani A, et al. The Mfge8-α8β1-PTEN pathway regulates airway smooth muscle contraction in allergic inflammation [published online May 15, 2018]. *FASEB J*. https://doi.org/10.1096/fj.201800109R.
23. Stricker J, et al. Spatiotemporal constraints on the force-dependent growth of focal adhesions. *Biophys J*. 2011;100(12):2883–2893.
24. Tang DD. Critical role of actin-associated proteins in smooth muscle contraction, cell proliferation, airway hyperresponsiveness and airway remodeling. *Respir Res*. 2015;16(1):134.
25. Yeh Y-C, et al. Mechanotransduction of matrix stiffness in regulation of focal adhesion size and number: reciprocal regulation of caveolin-1 and β1 integrin. *Sci Rep*. 2017;7(1):1–14.
26. Polio SR, et al. Extracellular matrix stiffness regulates human airway smooth muscle contraction by altering the cell-cell coupling. *Sci Rep*. 2019;9(1):1–12.
27. Wang T, et al. Recruitment of β-catenin to N-cadherin is necessary for smooth muscle contraction. *J Biol Chem*. 2015;290(14):8913–8924.
28. Buckley CD, et al. Cell adhesion. The minimal cadherin-catenin complex binds to actin filaments under force. *Science*. 2014;346(6209):1254211.
29. Sugimoto K, et al. The αvβ6 integrin modulates airway hyperresponsiveness in mice by regulating intraepithelial mast cells. *J Clin Invest*. 2012;122(2):748–758.
30. Kudo M, et al. Mfge8 suppresses airway hyperresponsiveness in asthma by regulating smooth muscle contraction. *Proc Natl Acad Sci U S A*. 2013;110(2):660–665.
31. Emsley J, et al. Structural basis of collagen recognition by integrin alpha2beta1. *Cell*. 2000;101(1):47–56.
32. Etoh T, et al. Role of integrin alpha 2 beta 1 (VLA-2) in the migration of human melanoma cells on laminin and type IV collagen. *J Invest Dermatol*. 1993;100(5):640–647.
33. Polacheck WJ, Chen CS. Measuring cell-generated forces: a guide to the available tools. *Nat Methods*. 2016;13(5):415–423.
34. Hall SL, et al. IL-17A enhances IL-13 activity by enhancing IL-13-induced STAT6 activation. *J Allergy Clin Immunol*. 2017;139(2):462–471.
35. Kay AB, et al. A role for eosinophils in airway remodelling in asthma. *Trends Immunol*. 2004;25(9):477–482.
36. Tepper RI, et al. IL-4 induces allergic-like inflammatory disease and alters T cell development in transgenic mice. *Cell*. 1990;62(3):457–467.
37. Wills-Karp M, et al. Interleukin-13: central mediator of allergic asthma. *Science*. 1998;282(5397):2258–2261.
38. Kudo M, et al. IL-17A produced by αβ T cells drives airway hyper-responsiveness in mice and enhances mouse and human airway smooth muscle contraction. *Nat Med*. 2012;18(4):547–554.
39. Busse WW, et al. Randomized, double-blind, placebo-controlled study of brodalumab, a human anti-IL-17 receptor monoclonal antibody, in moderate to severe asthma. *Am J Respir Crit Care Med*. 2013;188(11):1294–1302.
40. Hanania NA, et al. Efficacy and safety of lebrikizumab in patients with uncontrolled asthma (LAVOLTA I and LAVOLTA II): replicate, phase 3, randomised, double-blind, placebo-controlled trials. *Lancet Respir Med*. 2016;4(10):781–796.
41. Panettieri RA, et al. Tralokinumab for severe, uncontrolled asthma (STRATOS 1 and STRATOS 2): two randomised, double-blind, placebo-controlled, phase 3 clinical trials. *Lancet Respir Med*.

2018;6(7):511–525.
42. FitzGerald JM, et al. Benralizumab, an anti-interleukin-5 receptor α monoclonal antibody, as add-on treatment for patients with severe, uncontrolled, eosinophilic asthma (CALIMA): a randomised, double-blind, placebo-controlled phase 3 trial. *Lancet*. 2016;388(10056):2128–2141.
43. Castro M, et al. Dupilumab efficacy and safety in moderate-to-severe uncontrolled asthma. *N Engl J Med*. 2018;378(26):2486–2496.
44. Sears MR, Lötvall J. Past, present and future--beta2-adrenoceptor agonists in asthma management. *Respir Med*. 2005;99(2):152–170.
45. Breuer J, et al. VLA-2 blockade in vivo by vatelizumab induces CD4+FoxP3+ regulatory T cells. *Int Immunol*. 2019;31(6):407–412.
46. Mozaffari S, et al. Inflammatory bowel disease therapies discontinued between 2009 and 2014. *Expert Opin Investig Drugs*. 2015;24(7):949–956.
47. Milojkovic Kerklaan B, et al. A phase I, dose escalation, pharmacodynamic, pharmacokinetic, and food-effect study of α2 integrin inhibitor E7820 in patients with advanced solid tumors. *Invest New Drugs*. 2016;34(3):329–337.
48. Nieswandt B, et al. Glycoprotein VI but not alpha-2beta1 integrin is essential for platelet interaction with collagen. *EMBO J*. 2001;20(9):2120–2130.
49. Holtkötter O, et al. Integrin α2-deficient mice develop normally, are fertile, but display partially defective platelet interaction with collagen. *J Biol Chem*. 2002;277(13):10789–10794.
50. Alexander MS, et al. CD82 is a marker for prospective isolation of human muscle satellite cells and is linked to muscular dystrophies. *Cell Stem Cell*. 2016;19(6):800–807.
51. Schöber S, et al. The role of extracellular and cytoplasmic splice domains of alpha7-integrin in cell adhesion and migration on laminins. *Exp Cell Res*. 2000;255(2):303–313.
52. Zeltz C, et al. α11β1 integrin is induced in a subset of cancer-associated fibroblasts in desmoplastic tumor stroma and mediates in vitro cell migration. *Cancers (Basel)*. 2019;11(6):765.
53. Magness ST, et al. A dual reporter gene transgenic mouse demonstrates heterogeneity in hepatic fibrogenic cell populations. *Hepatology*. 2004;40(5):1151–1159.
54. Chen C, et al. ADAM33 is not essential for growth and development and does not modulate allergic asthma in mice. *Mol Cell Biol*. 2006;26(18):6950–6956.